Tenth International Conference on Computational Fluid Dynamics (ICCFD10), Barcelona,Spain, July 9-13, 2018

ICCFD10-2018-320

Setting up the Intrusive Polynomial Chaos Method for Uncertainty Quantification and Adjoint-based Optimization in Compressible Fluid Flows

M. Chatzimanolakis, K.-D. Kantarakias, V.G. Asouti and K.C. Giannakoglou
Corresponding author: kyr.kantar@gmail.com

Abstract: This paper presents an intrusive Polynomial Chaos Expansion (iPCE) method for uncertainty quantification and design/optimization under uncertainties in problems governed by the compressible fluid flow equations. For the optimization, a gradient–based algorithm is used, after developing the iPCE of the continuous adjoint method. A generalized mathematical framework leading to the numerical solution scheme of the primal and adjoint equations is implemented and ways to reduce the overall computational burden and memory requirements are proposed. Uncertainty quantification and shape optimization problems under uncertainties associated with the infinite flow conditions in external aerodynamics are demonstrated.

Keywords: Intrusive Polynomial Chaos, Uncertainty Quantification, Continuous Adjoint Method, Optimization Under Uncertainties.

1 Introduction

For the solution of flow problems under uncertainties, the (occasionally) very high computational cost of CFD evaluations makes stochastic sampling, such as standard Monte–Carlo methods [1], extremely expensive and, thus, unaffordable for real–world applications. As a consequence, a lot of research has been redirected towards developing other much more efficient Uncertainty Quantification (UQ) techniques, such as those based on Polynomial Chaos Expansions (PCE) [2, 3]. The PCE relies upon the spectral representation of the uncertain input to and/or output from the evaluation model [4, 5, 6, 7, 8, 9]. Apart from the UQ itself, optimization under uncertainties is profiting a lot from this kind of methods.

The straightforward implemention of the PCE is the so–called non–intrusive (niPCE) [10, 11, 12] one, that requires running the CFD code as a black–box at a number of points (Gaussian nodes, as defined by the Gauss Quadrature, GQ, integration rules). This method, though affordable in terms of computational cost compared to stochastic sampling, suffers from the curse of dimensionality as the number of uncertain variables increases. In the intrusive PCE (iPCE) [8, 4], the governing equations are altered through the spectral representation of their variables in an orthonormal stochastic space and undergo Galerkin projections leading to a new set of coupled equations which must be numerically solved. The major burden is, thus, the derivation of the iPCE equations and (the usually extensive) restructuring of the CFD software. Over and above, for each change in the number of uncertain variables, governing equations must be developed anew and additional programming is required, unless special care is taken; this is where this paper is focusing on, by addressing not only the solution of the UQ problem but, also, the corresponding adjoint–based optimization. In the literature, hybrid and semi–intrusive methods [13, 14, 15], combining the advantages of both approaches, can be found as a possible remedy to the aforementioned issue.

Once an efficient UQ method becomes available, the objective function, to be maximized or minimized during the optimization, must be defined. For the optimization itself, both stochastic and gradient-based methods can be used. Working with a stochastic method, for instance evolutionary algorithms (EAs), the UQ tool

is used as a black–box within the EA [16, 17]. Usually, emphasis is laid on the reduction of the number of evaluations required by the EA and the best way to do so is by means of surrogate evaluation models.

On the other side, in applications governed by (systems of) PDEs, gradient–based methods are assisted by the adjoint method for the computation of the gradients. One may combine the PCE with the adjoint method; by doing so, the spectral coefficients not only of the quantity of interest but of its gradients too can be computed and used with a gradient–based method for the design under uncertainties. In the literature, such applications use either non–intrusive, [18], or partially intrusive, [19], approaches for the adjoint method. This paper presents an efficient methodology for the development of the iPCE to the Navier–Stokes equations and their adjoint equations which can be used for any number of uncertain variables without formulating a different system of equations or changing the software. Numerical tricks for reducing the computational cost and memory requirements of the iPCE are described. The proposed algorithm is herein applied to shape optimization problems of airfoils with uncertain infinite flow conditions. Starting point for the programming was an Euler/Navier–Stokes solver for unstructured grids [20], based on a finite–volume discretization and vertex–centered storage.

2 The Flow Model and the iPCE Equations

The flow model used in this work is based on the Navier–Stokes equations for compressible fluids, namely

$$\boldsymbol{R}(\boldsymbol{U}) = \frac{\partial \boldsymbol{U}}{\partial t} + \frac{\partial \boldsymbol{f}_i^{inv}}{\partial x_i} - \frac{\partial \boldsymbol{f}_i^{vis}}{\partial x_i} = \boldsymbol{0} \tag{1}$$

where

$$\boldsymbol{f}_i^{inv} = \begin{pmatrix} \rho u_i \\ \rho u_i \boldsymbol{v} + p\boldsymbol{\delta}_i \\ v_i(E_t + p) \end{pmatrix} \ , \ \boldsymbol{f}_i^{vis} = \begin{pmatrix} 0 \\ \boldsymbol{\tau}_i \\ v_j \tau_{ij} + q_i \end{pmatrix} \tag{2}$$

are the inviscid and viscous flux vectors, q_i are the thermal flux components, $\boldsymbol{\delta}_i = (\delta_{i1}, \delta_{i2}, \delta_{i3})^T$, δ_{ij} is Kronecker's symbol and $\boldsymbol{\tau}_i = (\tau_{i1}, \tau_{i2}, \tau_{i3})^T$ the viscous stresses. The flow variables array is $\boldsymbol{U} = (\rho, \rho\boldsymbol{v}, E_t)^T$, with ρ the density, $\boldsymbol{v} = (v_1, v_2, v_3)^T$ the velocity vector, $E_t = \frac{p}{(\gamma-1)} - \frac{1}{2}\rho\, \boldsymbol{v}^2$ the total energy per unit volume and p the pressure.

Inviscid fluxes are expressed in terms of their Jacobians as $\boldsymbol{f}_i^{inv} = A_i \boldsymbol{U}, A_i = \frac{\partial \boldsymbol{f}_i^{inv}}{\partial \boldsymbol{U}}$ and the state equation of perfect gases is assumed. A vertex–centered finite–volume formulation is used and the equations are discretized on unstructured grids through the Flux Vector Splitting (FVS) technique.

To account for the uncertainties, a set of m uncorrelated stochastic variables $\boldsymbol{\xi} = (\xi_1, \ldots, \xi_m)$, each with its own probability density function $w_i(\xi_i)$ defined in the domain $\mathcal{E}_i$ is assumed to affect the flow through the boundary conditions. According to the iPCE theory, the flow variables are expanded using a polynomial basis Y which is orthonormal in $\mathcal{E} := \prod_{i=1}^m \mathcal{E}_i$ with respect to $W := \prod_{i=1}^m w_i$, as follows

$$\boldsymbol{U}(\boldsymbol{\xi}) = \sum_{i=0}^{q} \boldsymbol{U}^i Y_i(\boldsymbol{\xi}) \tag{3}$$

where $q+1 = \frac{(m+C)!}{m!C!}$ terms are retained in the truncated eq. 3. C denotes the user–defined chaos order [3]. The spectral coefficients $\boldsymbol{U}^i$ are defined through Galerkin projections as

$$\boldsymbol{U}^i = \int_{\mathcal{E}} \boldsymbol{U} Y_i W d\boldsymbol{\xi} \tag{4}$$

and, in the intrusive approach, their computation requires the numerical solution of the iPCE equations which are symbolically expressed as

$$\mathrm{G}^{\mathrm{q}}\left[\boldsymbol{R}(\boldsymbol{U})\right] = \boldsymbol{0} \tag{5}$$

Hereafter the Galerkin operator $\mathrm{G}^{\mathrm{q}}[.]$ will be denoted by $\mathrm{G}[.]$. The latter is applied to scalars, vectors or matrices. For a scalar $\phi(\boldsymbol{\xi})$, $\mathrm{G}[\phi] = (\phi^0, \phi^1, \ldots, \phi^q)^T$. For a vector $\boldsymbol{U}(\boldsymbol{\xi}) = (U_1(\boldsymbol{\xi}), \ldots, U_n(\boldsymbol{\xi}))^T$ with

$U_i = \sum_{k=0}^{q} U_i^k Y_k(\boldsymbol{\xi})$, $\mathrm{G}[\boldsymbol{U}] = (\boldsymbol{U}^0, \boldsymbol{U}^1, \ldots, \boldsymbol{U}^q)^T$, where $\boldsymbol{U}^k = (U_1^k, \ldots, U_n^k)$, superscripts denote the spectral components and subscripts the U components. Finally, for a matrix $A \in \mathbb{R}^{n\times n}$ with components $A_{ij} = \sum_{k=0}^{q} A_{ij}^k Y_k(\boldsymbol{\xi})$ this operation yields

$$\mathrm{G}[A] = \begin{bmatrix} A^{00} & A^{01} & \ldots & A^{0q} \\ A^{10} & A^{11} & \ldots & A^{1q} \\ \vdots & \vdots & \vdots & \vdots \\ A^{q0} & A^{q1} & \ldots & A^{qq} \end{bmatrix}$$

with the (i,j) element of the $A^{\lambda\mu} \in \mathbb{R}^{n\times n}$ block given by $A_{ij}^{\lambda\mu} := \int_{\mathcal{E}} A_{ij} Y_\lambda Y_\mu W d\boldsymbol{\xi}$.

2.1 Numerical Solution of the iPCE equations

In the problem without uncertainties, let $\boldsymbol{R}(\boldsymbol{U})=\boldsymbol{0}$ denote the flow equations, with the values of $\boldsymbol{U}$ at each mesh node as the unknowns. This non–linear system is solved for $\Delta\boldsymbol{U}$ through the iterative scheme

$$\left(\frac{\partial \boldsymbol{R}}{\partial \boldsymbol{U}}\right)_{old} \Delta\boldsymbol{U} = -\boldsymbol{R}_{old}, \qquad \boldsymbol{U}_{new} = \boldsymbol{U}_{old} + \Delta\boldsymbol{U} \tag{6}$$

In the presence of uncertainties, by applying the $\mathrm{G}[.]$ operator (index 'old' is omitted hereafter) we get

$$\mathrm{G}\left[\frac{\partial \boldsymbol{R}}{\partial \boldsymbol{U}}\Delta\boldsymbol{U}\right] = -\mathrm{G}[\boldsymbol{R}], \qquad \mathrm{G}[\boldsymbol{U}_{new}] = \mathrm{G}[\boldsymbol{U}] + \mathrm{G}[\Delta\boldsymbol{U}] \tag{7}$$

It can be shown that for any matrix A and vector $\boldsymbol{x}$

$$\mathrm{G}[A\ \boldsymbol{x}] = \mathrm{G}[A]\,\mathrm{G}[\boldsymbol{x}] \tag{8}$$

which results to

$$\mathrm{G}\left[\frac{\partial \boldsymbol{R}}{\partial \boldsymbol{U}}\right] \mathrm{G}[\Delta\boldsymbol{U}] = -\mathrm{G}[\boldsymbol{R}] \tag{9}$$

Eq. 9 is solved iteratively for $\mathrm{G}[\Delta\boldsymbol{U}]$, as $\mathrm{G}[\boldsymbol{U}]$ are the unknowns of the iPCE equations. We are, thus, setting up an iterative solver for the iPCE equations without first deriving them. Regarding the LHS matrix in eq. 9, the Galerkin projection of the flow Jacobian is equal to the Jacobian of $\mathrm{G}[\boldsymbol{R}]$ with respect to $\mathrm{G}[\boldsymbol{U}]$, or

$$\mathrm{G}\left[\frac{\partial \boldsymbol{R}}{\partial \boldsymbol{U}}\right] = \frac{\partial(\mathrm{G}[\boldsymbol{R}])}{\partial(\mathrm{G}[\boldsymbol{U}])} \tag{10}$$

To prove eq. 10 one may first show that, for any scalar field ϕ,

$$\frac{\partial \phi}{\partial \boldsymbol{U}^\lambda} = \frac{\partial \phi}{\partial \boldsymbol{U}^\lambda}\,\frac{\partial \boldsymbol{U}}{\partial \boldsymbol{U}^\lambda} \overset{eq.3}{=} Y_\lambda\,\frac{\partial \phi}{\partial \boldsymbol{U}} \tag{11}$$

Because of eq. 11, the (i,j) element of the (λ,μ) block of matrix $\mathrm{G}\left[\frac{\partial \boldsymbol{R}}{\partial \boldsymbol{U}}\right]$ is

$$\left(\frac{\partial \boldsymbol{R}}{\partial \boldsymbol{U}}\right)_{ij}^{\lambda\mu} = \int_{\mathcal{E}} Y_\lambda Y_\mu \left(\frac{\partial \boldsymbol{R}}{\partial \boldsymbol{U}}\right)_{ij} W d\boldsymbol{\xi} \overset{eq.4}{=} \int_{\mathcal{E}} Y_\mu \frac{\partial R_i}{\partial U_j^\lambda} W d\boldsymbol{\xi} = \left(\frac{\partial R_i}{\partial U_j^\lambda}\right)^\mu = \frac{\partial R_i^\mu}{\partial U_j^\lambda}$$

Thanks to eq. 10, computing the Jacobian of the discrete iPCE equations solely requires the Jacobian of the problem without uncertainties. Upon the numerical solution of the iPCE equations, the Quantity of Interest (QoI), denoted by F, can also be expanded as

$$F(\boldsymbol{\xi}) = \sum_{i=0}^{q} F^i Y_i(\boldsymbol{\xi}) \tag{12}$$

so that its mean value and standard deviation become

$$\mu_F = F^0 \ , \qquad \sigma_F = \sqrt{\sum_{i=1}^{q} (F^i)^2} \tag{13}$$

The spectral coefficients F^i are found by the Galerkin projections of the QoI, which in turn requires the known spectral coefficients of $\boldsymbol{U}$.

2.2 Reducing Computational Cost & Memory Requirements of the iPCE Solver

In the iPCE problem, the involved LHS matrices are now of much larger dimensions ($(q+1)^2$ times larger) than their deterministic counterparts and this noticeably increases memory requirements. To keep the memory footprint of the iPCE solver as low as possible, the following treatment is proposed. Let $\boldsymbol{\xi}_z$ be the vector formed by the roots of all orthonormal polynomials Y_i of first degree. Then, $\boldsymbol{U}^0$ is approximated by $\boldsymbol{U}(\boldsymbol{\xi} = \boldsymbol{\xi}_z)$, which is obtained through the solution of eq. 1 for the problem without uncertainties. If, for instance, uncertainties are related to the flow conditions, the $\boldsymbol{\xi}_z$ values determine the flow conditions at which the equations should be solved to approximate $\boldsymbol{U}^0$. The error of this approximation is relatively small since

$$\boldsymbol{U}(\boldsymbol{\xi}_z) - \boldsymbol{U}^0 = \sum_{i=0}^{\infty} \boldsymbol{U}^i Y_i(\boldsymbol{\xi}_z) - \boldsymbol{U}^0 = \underbrace{\sum_{i=1}^{q_2-1} \boldsymbol{U}^i Y_i(\boldsymbol{\xi}_z)}_{=0} + \sum_{i=q_2}^{\infty} \boldsymbol{U}^i Y_i(\boldsymbol{\xi}_z) \tag{14}$$

where $q_2 = \frac{(m+2)!}{2!m!}$. For $C=1$, eq. 9 is written as

$$\begin{bmatrix} \frac{\partial \boldsymbol{R}^{00}}{\partial \boldsymbol{U}} & \frac{\partial \boldsymbol{R}^{01}}{\partial \boldsymbol{U}} & \frac{\partial \boldsymbol{R}^{02}}{\partial \boldsymbol{U}} & \cdots & \frac{\partial \boldsymbol{R}^{0q_1}}{\partial \boldsymbol{U}} \\ \frac{\partial \boldsymbol{R}^{10}}{\partial \boldsymbol{U}} & \frac{\partial \boldsymbol{R}^{00}}{\partial \boldsymbol{U}} & \boldsymbol{0} & \cdots & \boldsymbol{0} \\ \frac{\partial \boldsymbol{R}^{20}}{\partial \boldsymbol{U}} & \boldsymbol{0} & \frac{\partial \boldsymbol{R}^{00}}{\partial \boldsymbol{U}} & \cdots & \boldsymbol{0} \\ \vdots & \vdots & \vdots & \vdots & \vdots \\ \frac{\partial \boldsymbol{R}^{q_1 0}}{\partial \boldsymbol{U}} & \boldsymbol{0} & \boldsymbol{0} & \cdots & \frac{\partial \boldsymbol{R}^{00}}{\partial \boldsymbol{U}} \end{bmatrix} \begin{bmatrix} \Delta \boldsymbol{U}^0 \\ \Delta \boldsymbol{U}^1 \\ \Delta \boldsymbol{U}^2 \\ \vdots \\ \Delta \boldsymbol{U}^{q_1} \end{bmatrix} = - \begin{bmatrix} \boldsymbol{R}^0 \\ \boldsymbol{R}^1 \\ \boldsymbol{R}^2 \\ \vdots \\ \boldsymbol{R}^{q_1} \end{bmatrix} \tag{15}$$

because $< Y_\rho, Y_\lambda, Y_\mu >= \delta_{0\rho}\delta_{\lambda\mu}$, $1 \leq \lambda,\ \mu \leq q_1$, $0 \leq \rho \leq q_1$, where q_1 is defined by setting $C=1$ in the definition of q, i.e. $q_1 = m$ and δ_{ij} is the Kronecker symbol. Moreover, since $\boldsymbol{U}^0$ is well–approximated, $\Delta U^0 \approx \boldsymbol{0}$. This justifies the decision to keep only the diagonal blocks in eq. 15, which are all equal to each other. As a result, for $C=1$, the equations are solved by keeping only the diagonal of the Jacobian approximated as

$$\frac{\partial \boldsymbol{R}^{00}}{\partial \boldsymbol{U}} \approx \left. \frac{\partial \boldsymbol{R}}{\partial \boldsymbol{U}} \right|_{\boldsymbol{U}=\boldsymbol{U}(\boldsymbol{\xi}_z)} \tag{16}$$

and obtained by solving the problem without uncertainties at $\boldsymbol{\xi} = \boldsymbol{\xi}_z$.
For $C>1$, the solution process is quite similar since the (constant) diagonal block is retained on the extra rows as well. Moreover, the solution for $C=1$ can be used to initialize the remaining coefficient fields $\boldsymbol{U}^k$, in order to facilitate convergence if $C=2$. If $C=3$, the solution fields to the equations for $C=2$ are used for the subsequent initializations and so forth.

3 The Adjoint iPCE Formulation

This section proposes a way to derive the continuous adjoint equations of the primal iPCE problem presented in section 2, for use in aerodynamic shape optimization under uncertainties. Emphasis is laid on establishing a formulation which is easy to program, with just a reasonable amount of interventions in the existing adjoint code for the problem without uncertainties.

3.1 Continuous Adjoint Formulation without Uncertainties

Let us consider the following (primal) problem defined in a domain Ω with boundary S

$$\begin{array}{l} L\boldsymbol{U} - \boldsymbol{f} = \boldsymbol{0} \ , \text{ in } \Omega \\ B\boldsymbol{U} - \boldsymbol{e} = \boldsymbol{0} \ , \text{ on } S \end{array} \tag{17}$$

and a QoI given by

$$F = \int_S \boldsymbol{h}^T C\boldsymbol{U} dS \tag{18}$$

where L, B and C are linear differential operators; on the other hand $\boldsymbol{f}, \boldsymbol{e}$ and $\boldsymbol{h}$ may depend on the spatial coordinates x_i but not on the primal variables $\boldsymbol{U}$. Assuming the QoI is an objective function to be minimized/maximized constrained by eqs. 17, the augmented objective function

$$F_{aug} = F + \int_\Omega \boldsymbol{\Psi}^T (L\boldsymbol{U} - \boldsymbol{f}) d\Omega + \int_S (C^*\boldsymbol{\Psi})^T (B\boldsymbol{U} - \boldsymbol{e}) dS \tag{19}$$

is defined using the adjoint variables $\boldsymbol{\Psi}$. Let $\boldsymbol{b}$ denote the array of design variables, $\delta \equiv \delta/\delta\boldsymbol{b}$ the total derivative w.r.t. $\boldsymbol{b}$ and $\partial \equiv \partial/\partial\boldsymbol{b}$ the partial derivative representing variations due to changes in the design and flow variables excluding space deformations. In general,

$$\delta(C\boldsymbol{U}) = C(\delta\boldsymbol{U}) + (\delta C)\boldsymbol{U} \tag{20}$$

For instance, if $C \equiv \frac{\partial}{\partial x_i}$, then $\delta(C\boldsymbol{U}) = \frac{\partial(\delta\boldsymbol{U})}{\partial x_i} - \frac{\partial(\delta x_k)}{\partial x_i}\frac{\partial \boldsymbol{U}}{\partial x_k}$ hence $\delta C = -\frac{\partial(\delta x_k)}{\partial x_i}\frac{\partial()}{\partial x_k}$. Thus, the total derivative of the objective function F is

$$\delta F = \underbrace{\int_S \delta\boldsymbol{h}^T C\boldsymbol{U} dS + \int_S \boldsymbol{h}^T(\delta C)\boldsymbol{U} dS + \int_S \boldsymbol{h}^T C\boldsymbol{U}\delta(dS)}_{=:\delta F_{SD}} + \int_S \boldsymbol{h}^T C(\delta\boldsymbol{U}) dS \tag{21}$$

or that of the augmented function F_{aug}

$$\begin{aligned} \delta F_{aug} = \delta F_{SD} &+ \int_S \boldsymbol{h}^T C(\delta\boldsymbol{U}) dS + \int_\Omega \boldsymbol{\Psi}^T L(\delta\boldsymbol{U}) d\Omega + \int_S (C^*\boldsymbol{\Psi})^T B(\delta\boldsymbol{U}) dS \\ &+ \underbrace{\int_\Omega \boldsymbol{\Psi}^T[(\delta L)\boldsymbol{U} - \delta\boldsymbol{f}] d\Omega + \int_S (C^*\boldsymbol{\Psi})^T[(\delta B)\boldsymbol{U} - \delta\boldsymbol{e}] dS}_{=:\delta F_{SD}^{\Psi}} \end{aligned} \tag{22}$$

where terms indexed by SD contribute to the Sensitivity Derivatives. Integration by parts of the first volume integral on the RHS yields

$$\int_\Omega \boldsymbol{\Psi}^T L(\delta\boldsymbol{U}) d\Omega \equiv \int_\Omega (A\boldsymbol{\Psi})^T \delta\boldsymbol{U} d\Omega + \int_S (D\boldsymbol{\Psi})^T E(\delta\boldsymbol{U}) dS \tag{23}$$

where A, D and E are appropriate differential operators depending on L. Then, eq. 22 is rewritten as

$$\begin{aligned} \delta F_{aug} = \delta F_{SD} + \delta F_{SD}^{\Psi} &+ \int_\Omega (A\boldsymbol{\Psi})^T \delta\boldsymbol{U} d\Omega + \int_S (\boldsymbol{h} - B^*\boldsymbol{\Psi})^T C(\delta\boldsymbol{U}) dS \\ &+ \underbrace{\int_S (C^*\boldsymbol{\Psi})^T B(\delta\boldsymbol{U}) dS + \int_S (B^*\boldsymbol{\Psi})^T C(\delta\boldsymbol{U}) dS + \int_S (D\boldsymbol{\Psi})^T E(\delta\boldsymbol{U}) dS}_{=:M} \end{aligned} \tag{24}$$

where B^* is a newly introduced differential operator which facilitates the expression of the adjoint boundary conditions. Both B^* and C^* are determined by setting M to zero, giving rise to the adjoint field equation,

the adjoint boundary conditions

$$\begin{array}{c} A\boldsymbol{\Psi} = \mathbf{0} \ , \ \text{in } \Omega \\ B^{*}\boldsymbol{\Psi} = \boldsymbol{h} \ , \ \text{on } S \end{array} \tag{25}$$

as well as the expression of the gradient of F

$$\delta F = \delta F_{SD} + \delta F_{SD}^{\Psi} \tag{26}$$

3.2 The Continuous Adjoint iPCE Problem

In the presence of uncertainties, the primal equations are

$$\begin{array}{c} \mathrm{G}\left[L\boldsymbol{U} - \boldsymbol{f}\right] = \mathbf{0} \ , \ \text{in } \Omega \\ \mathrm{G}\left[B\boldsymbol{U} - \boldsymbol{e}\right] = \mathbf{0} \ , \ \text{on } S \end{array} \tag{27}$$

and the objective function J of the problem is defined as a linear combination of the absolute values of the spectral coefficients F^i of the QoI

$$J := \sum_{i=0}^{q} \zeta_i |F^i| = \sum_{i=0}^{q} \underbrace{\zeta_i sign(F^i)}_{\zeta^i} F^i \tag{28}$$

where ζ^i are user–defined weights. By considering ζ^i to be the spectral coefficients of a stochastic quantity

$$\zeta(\boldsymbol{\xi}) = \sum_{i=0}^{q} \zeta^i Y_i(\boldsymbol{\xi}) \tag{29}$$

the objective function to be minimized becomes

$$J = \sum_{i=0}^{q} \zeta^i F^i = \mathrm{G}\left[\zeta\right]^T \mathrm{G}\left[F\right] \tag{30}$$

Similarly to the case without uncertainties, we define

$$J_{aug} := J + \int_{\Omega} \mathrm{G}\left[\underset{\sim}{\boldsymbol{\Psi}}\right]^T \mathrm{G}\left[L\boldsymbol{U} - \boldsymbol{f}\right] d\Omega + \int_{S} \mathrm{G}\left[\underset{\sim}{C^{*}\boldsymbol{\Psi}}\right]^T \mathrm{G}\left[B\boldsymbol{U} - \boldsymbol{e}\right] dS \tag{31}$$

where the new adjoint fields ($\mathrm{G}\left[\underset{\sim}{\boldsymbol{\Psi}}\right]$, $\mathrm{G}\left[\underset{\sim}{C^{*}\boldsymbol{\Psi}}\right]$) introduced in eq. 31 are considered to be the Galerkin projections of two stochastic fields $\underset{\sim}{\boldsymbol{\Psi}}$ and $\underset{\sim}{C^{*}\boldsymbol{\Psi}}$. For the sake of simplicity, symbol $\sim$ will hereafter be omitted. Since $\delta()$ and $\mathrm{G}\left[.\right]$ permute, the total derivative of J is given by

$$\delta J = \delta(\mathrm{G}\left[\zeta\right]^T \mathrm{G}\left[F\right]) = \mathrm{G}\left[\zeta\right]^T \left(\mathrm{G}\left[\delta F_{SD}\right] + \int_{S} \mathrm{G}\left[\boldsymbol{h}^T C(\delta \boldsymbol{U})\right] dS \right) \tag{32}$$

Based on the above, the total derivative of J_{aug} becomes

$$\begin{aligned} \delta J_{aug} &= \delta J + \int_{\Omega} \mathrm{G}\left[\boldsymbol{\Psi}\right]^T \mathrm{G}\left[L(\delta \boldsymbol{U})\right] d\Omega + \int_{S} \mathrm{G}\left[C^{*}\boldsymbol{\Psi}\right]^T \mathrm{G}\left[B(\delta \boldsymbol{U})\right] dS \\ &\quad + \int_{\Omega} \mathrm{G}\left[\boldsymbol{\Psi}\right]^T \mathrm{G}\left[(\delta L)\boldsymbol{U} - \delta \boldsymbol{f}\right] d\Omega + \int_{S} \mathrm{G}\left[C^{*}\boldsymbol{\Psi}\right]^T \mathrm{G}\left[(\delta B)\boldsymbol{U} - \delta \boldsymbol{e}\right] dS \overset{eq.32}{=} \\ &= \mathrm{G}\left[\zeta\right]^T \mathrm{G}\left[\delta F_{SD}\right] + \int_{S} \mathrm{G}\left[\zeta \boldsymbol{h}\right]^T \mathrm{G}\left[C(\delta \boldsymbol{U})\right] dS + \int_{\Omega} \mathrm{G}\left[\boldsymbol{\Psi}\right]^T \mathrm{G}\left[L(\delta \boldsymbol{U})\right] d\Omega \\ &\quad + \int_{S} \mathrm{G}\left[C^{*}\boldsymbol{\Psi}\right]^T \mathrm{G}\left[B(\delta \boldsymbol{U})\right] dS + \mathrm{G}\left[\delta F_{SD}^{\Psi}\right]^T \mathrm{G}\left[1\right] \end{aligned} \tag{33}$$

where $\mathrm{G}\left[1\right] = [1, 0, \ldots, 0]^T$. Through integration by parts and since $\mathrm{G}\left[A\boldsymbol{U}\right] = \mathrm{G}\left[A\right]\mathrm{G}\left[\boldsymbol{U}\right]$, we get

$$\int_\Omega \mathrm{G}\left[\boldsymbol{\Psi}\right]^T \mathrm{G}\left[L(\delta\boldsymbol{U})\right] d\Omega = \int_\Omega \mathrm{G}\left[A\boldsymbol{\Psi}\right]^T \mathrm{G}\left[\delta\boldsymbol{U}\right] d\Omega + \int_S \mathrm{G}\left[D\boldsymbol{\Psi}\right]^T \mathrm{G}\left[E(\delta\boldsymbol{U})\right] dS \tag{34}$$

Then, eq. 33 is written

$$\begin{aligned}\delta J_{aug} = {} & \mathrm{G}\left[\zeta\right]^T \mathrm{G}\left[\delta F_{SD}\right] + \mathrm{G}\left[\delta F_{SD}^{\Psi}\right]^T \mathrm{G}\left[1\right] \\ & + \int_\Omega \mathrm{G}\left[A\boldsymbol{\Psi}\right]^T \mathrm{G}\left[\delta\boldsymbol{U}\right] d\Omega + \int_S \mathrm{G}\left[\zeta\boldsymbol{h} - B^*\boldsymbol{\Psi}\right]^T \mathrm{G}\left[C(\delta\boldsymbol{U})\right] dS \\ & + \underbrace{\int_S \mathrm{G}\left[C^*\boldsymbol{\Psi}\right]^T \mathrm{G}\left[B(\delta\boldsymbol{U})\right] dS + \int_S \mathrm{G}\left[D\boldsymbol{\Psi}\right]^T \mathrm{G}\left[E(\delta\boldsymbol{U})\right] dS + \int_S \mathrm{G}\left[B^*\boldsymbol{\Psi}\right]^T \mathrm{G}\left[C(\delta\boldsymbol{U})\right] dS}_{=\mathrm{G}[M]^T\,\mathrm{G}[1]}\end{aligned} \tag{35}$$

Operators B^* and C^* are determined by setting $\mathrm{G}\left[M\right]^T \mathrm{G}\left[1\right]$ to zero. Note that, in such a case, B^* and C^* will be identical to those of the case without uncertainties. Starting from eq. 35, $\boldsymbol{\Psi}$ ($\underset{\sim}{\boldsymbol{\Psi}}$, in fact) must satisfy the adjoint iPCE equation and the adjoint boundary conditions,

$$\begin{aligned}&\mathrm{G}\left[A\boldsymbol{\Psi}\right] = \boldsymbol{0}\ ,\ \text{in } \Omega \\ &\mathrm{G}\left[B^*\boldsymbol{\Psi}\right] = \mathrm{G}\left[\zeta\boldsymbol{h}\right]\ ,\ \text{on } S\end{aligned} \tag{36}$$

whereas

$$\delta J = \mathrm{G}\left[\zeta\right]^T \mathrm{G}\left[\delta F_{SD}\right] + \mathrm{G}\left[\delta F_{SD}^{\Psi}\right]^T \mathrm{G}\left[1\right] \tag{37}$$

Eq. 36 implies that the field adjoint equations to the iPCE primal problem result from the Galerkin projections of eq. 25. The imposed adjoint boundary conditions are though different since these now include ζ, defined in eq. 29. Eq. 37 is also quite similar to eq. 26, as it involves the Galerkin projections of its terms.

3.3 Programming Issues

The numerical solution of the adjoint iPCE equation is carried out in a similar manner to that of the primal problem. The iterative scheme is written as

$$\mathrm{G}\left[\frac{\partial \boldsymbol{R}^{\Psi}}{\partial \boldsymbol{\Psi}}\right] \mathrm{G}\left[\Delta\boldsymbol{\Psi}\right] = -\,\mathrm{G}\left[\boldsymbol{R}^{\Psi}\right] \tag{38}$$

where $\boldsymbol{R}^{\Psi} = A\boldsymbol{\Psi}$. Eq. 38 is solved similarly to the iPCE equations, i.e. by keeping only the diagonal blocks on the LHS. For the RHS, the computation of $\boldsymbol{R}^{\Psi}$ is required, which is based on the same routines used in the problem without uncertainties; there is a slight difference though: without uncertainties $\zeta = 1$, while in their presence ζ is given by eq. 29. For the initialization of $\boldsymbol{\Psi}$, the adjoint problem without uncertainties is solved by setting

$$\zeta = \zeta^0 = \zeta_0 sign(F^0) \tag{39}$$

corresponding to the solution of the adjoint iPCE equation for $C = 0$; $\Psi(\boldsymbol{\xi} = \boldsymbol{\xi}_z)$ is thus computed. The solution of the iPCE adjoint equations is followed by the computation of the sensitivity derivatives, eq. 37 for which existing routines are also used.

Finally, regarding the choice of weights ζ_i, two comments should be made. First, since $E[F] = F^0$ and $Var[F] = \sum_{i=1}^{q} (F^i)^2$, the magnitude of $|\zeta_0|$, compared to $|\zeta_i|, i \in [1, q]$ determines whether emphasis is laid on minimizing the mean value or the variance. Second, the signs of the coefficients are important. Without loss of generality, we may assume that J is to be minimized. Therefore, $\zeta_i > 0, i \in [1, q]$ since we are always interested in minimizing the variance. For instance, if F is to be minimized in the deterministic problem, ζ_0 will be positive.

4 Method Demonstration

The aforementioned iPCE methods are used for both UQ and shape optimization studies. In specific, a UQ around an aircraft configuration is initially presented with emphasis on the accuracy of the obtained results and the gain in computational cost of the iPCE compared to the non–intrusive PCE variant. Then, shape designs of a 2D isolated airfoil without and under uncertainties are carried out and the optimized solutions are compared.

4.1 UQ of the Inviscid Flow Around an Aircraft Configuration

The first case is concerned with the inviscid transonic flow around an aircraft configuration (practically the wing–fuselage configuration of DLR–F6 of [21], herein studied at inviscid flow conditions). The free–stream flow conditions are: $M_\infty = 0.75$ and $a_\infty = 0^o$ and the QoI is the lift coefficient C_L. Uncertain flow conditions are considered as follows

$$M_\infty \sim N(0.75, 0.02), \quad a_\infty \sim \mathcal{U}(-1^o, +1^o)$$

where $\mathcal{N}(a, b)$ denotes the normal distribution, with mean value a and standard deviation b and $\mathcal{U}(a, b)$ the uniform distribution in $[a, b]$. Note that the orthogonal polynomials used for these distributions are the Hermite and the Legendre polynomials, respectively.
UQ computations using both the iPCE and the niPCE approaches were carried out and the results are compared in table 1. Note that the CPU time is non–dimensionalized with the time of a single UQ computation on the same processor(s) using the proposed iPCE method. The mean value and the standard deviation of the Mach number around the aircraft is illustrated in fig. 1.
From table 1 it can be seen that the results of the iPCE and the niPCE for two uncertain variables are in full agreement and the proposed method is more efficient in terms of computational cost (about 50% faster for $C = 1$ and 40% for $C = 2$). This difference is attributed to the benefits of the method described in section 2.2. Namely, the well–chosen initialization of the mean flow field, along with the decoupling of the iPCE equations led to their convergence in 120 iterations of the point–implicit Jacobi solver, for $C = 1$, compared to the 160 iterations required for the niPCE. This is depicted in fig. 2, which shows the convergence of the spectral coefficients of the QoI as a function of the number of iterations.

	iPCE	niPCE	iPCE	niPCE
	$C=1$		$C=2$	
μ_{C_L}	0.47172	0.47172	0.47172	0.47172
σ_{C_L}	0.06661	0.06689	0.06694	0.06694
CPU time	1	1.941	1	1.598

Table 1: Inviscid flow around an aircraft configuration. Statistical moments of the lift coefficient computed using the iPCE and niPCE (with $C = 1, 2$) and the normalized computational cost of the two methods.

4.2 Shape Optimization of a 2D Airfoil – Laminar Flow

The second case deals with the shape optimization of a 2D isolated airfoil in the presence of uncertainties. The airfoil geometry is parameterized using two Bezier curves and the coordinates of their control points are the design variables.
Initially, a shape optimization without uncertainties is carried out. The fixed flow conditions are: $M_\infty = 0.5$, $a_\infty = 2^o$ and chord–based Reynolds number $Re = 6000$;the flow is laminar flow. The optimization aims at minimizing the drag coefficient (C_D), i.e. the objective function is $F = C_D$. The resulting optimized geometry yields a C_D value of about 20% smaller than that of the initial symmetric airfoil, fig. 3.

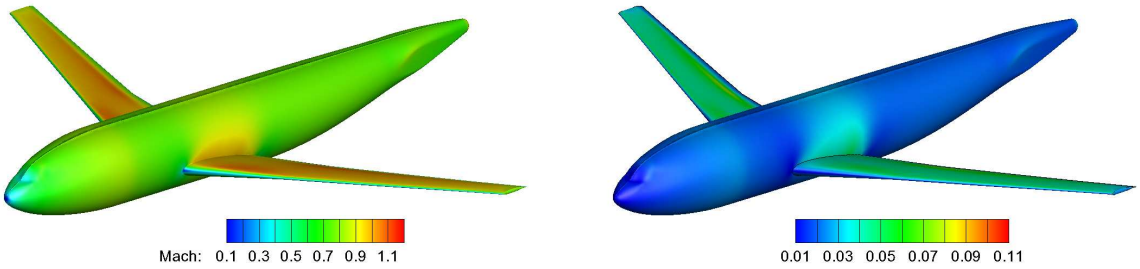

Figure 1: Inviscid flow around an aircraft configuration. Fields of the mean (left) and standard deviation (right) of the Mach number (iPCE, $C=1$), plotted on the aircraft surface.

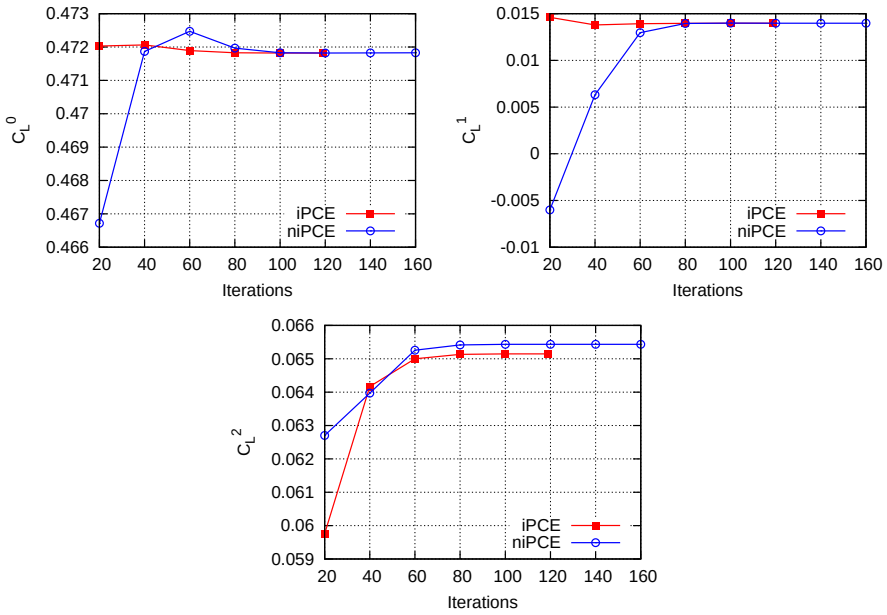

Figure 2: Inviscid flow around an aircraft configuration. Comparison of the convergence of the spectral coefficients of the lift coefficient (computed using iPCE and niPCE, $C=1$). Mean lift coefficient C_L^0 (top – left), spectral coefficients C_L^1 corresponding to M_∞(top – right) and C_L^2 corresponding to a_∞ (bottom).

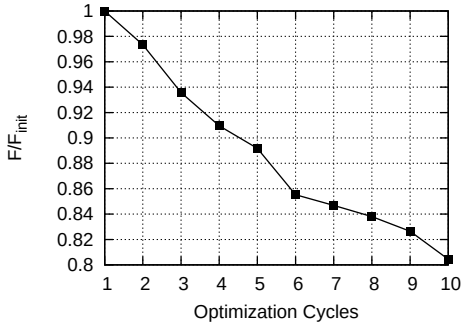

Figure 3: Shape optimization of a 2D airfoil; laminar flow. History of the objective function value in the optimization without uncertainties for min. drag.

Shape–optimization under uncertainties follows. Uncertainties are introduced in the flow conditions with the following probability distributions

$$M_\infty \sim \mathcal{N}(0.5, 0.05) \quad , \quad a_\infty \sim \mathcal{U}(1.5^o, 2.5^o) \quad , \quad Re \sim \mathcal{N}(6000, 250)$$

and the objective function is formulated as

$$J = \sum_{j=0}^{q} \zeta_j |F^j|$$

with $q=19$ (for $m=3$ uncertain variables and chaos order $C=3$), $\zeta_0=1$ and $\zeta_j=3 \; \forall \; j > 0$.
A reduction of the QoI of about 18% is achieved, see fig. 4. The optimized airfoil geometries resulted from the two runs (without and under uncertainties) compared to the initial one are shown in fig. 5. The fields of the adjoint velocity magnitude on the optimized geometries are illustrated in fig. 6. Table 2 compares the statistical moments of C_D from both optimization runs. The values on the left column are computed by a UQ run of the geometry resulted from the optimization run without uncertainties. As expected, the run without uncertainties yields lower mean value but has higher standard deviation.

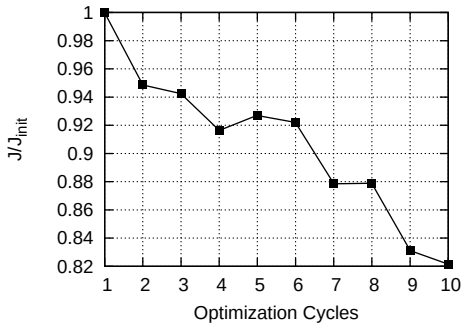

Figure 4: Shape optimization of a 2D airfoil; laminar flow. History of the objective function in the optimization under uncertainties.

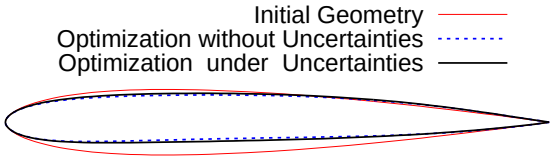

Figure 5: Shape optimization of a 2D airfoil; laminar flow. Comparison of the optimized geometries with and without uncertainties with the initial one.

	Without Uncertainties	Under Uncertainties
μ_{C_D}	$6.81 \cdot 10^{-2}$	$6.97 \cdot 10^{-2}$
σ_{C_D}	$1.11 \cdot 10^{-3}$	$1.05 \cdot 10^{-3}$

Table 2: Shape optimization of a 2D airfoil; laminar flow. Comparison of the statistical moments of the drag coefficient of the optimized geometries which resulted from the two runs.

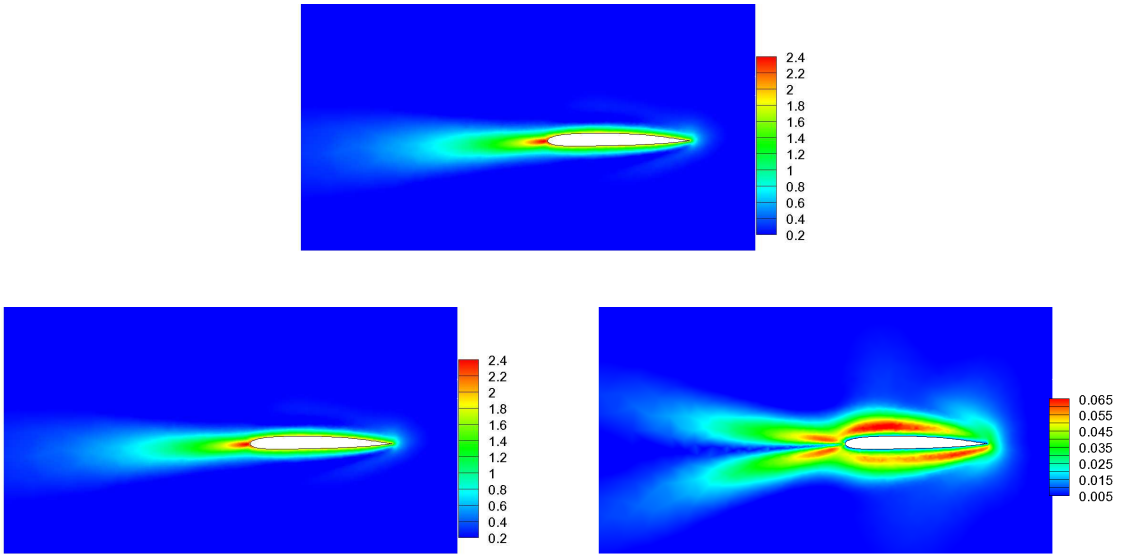

Figure 6: Shape optimization of a 2D airfoil; laminar flow. Field of the non–dimensional adjoint velocity magnitude computed by the design without uncertainties (top) and mean (bottom–left) and standard deviation of the adjoint velocity from the design under uncertainties.

5 Conclusions

This paper presented an intrusive Polynomial Chaos Expansion method for UQ and shape optimization under uncertainties. A generalized mathematical development for obtaining the iPCE to the Navier–Stokes equations and ways for reducing the computational cost and memory requirements were presented. To perform a gradient–based optimization, the adjoint to the iPCE equations has also been developed using the same mathematical framework. The great advantage of the proposed method is that (a) it can be formulated without first developing the PDEs governing the spectral fields of the flow variables and (b) the programming of both the primal and the adjoint code benefits, to the greatest extent, of the code for the problem without uncertainties. The proposed method was demonstrated in shape optimization problems under uncertainties associated with the infinite flow conditions in external aerodynamics. The optimal solutions from the design under uncertainties, as expected, are more robust compared to those found by the optimization without uncertainties.

References

[1] S. Asmussen and P.W. Glyn. *Stochastic Simulation: Algorithms and Analysis*. Springer, New York, 2007.

[2] N. Wiener. The homogeneous chaos. *American Journal of Mathematics*, 60:897–936, 1938.

[3] D. Xiu and G. Karniadakis. Modeling uncertainty in flow simulations via generalized polynomial chaos. *Journal of Computational Physics*, 187:37–67, 2003.

[4] M.P. Pettersson, G. Iaccarino, and J. Nordström. *Polynomial Chaos Methods for Hyperbolic Partial Differential Equations*. Springer International Publishing, Switzerland, 2015.

[5] O.P. Le Maître, O.M. Knio, H.N. Najm, and R.G. Ghanem. A stochastic projection method for fluid flow I. Basic formulation. *Journal of Computational Physics*, 173(2):481–511, 2001.

[6] B.J. Debusschere, H.N. Najm, P.P. Pébray, O.M. Knio, R.G. Ghanem, and O.P. Le Maître. Numerical challenges in the use of polynomial chaos representations for stochastic processes. *SIAM Journal of Scientific Computing*, 26(2):698–719, 2004.

[7] O.M. Knio and O.P. Le Maître. Uncertainty propagation in CFD using polynomial chaos decomposition. *Fluid Dynamics Research*, 38:616–640, 2006.

[8] C. Dinescu, S. Smirnov, C. Hirsch, and C. Lacor. Assessment of intrusive and non-intrusive non-deterministic CFD methodologies based on polynomial chaos expansions. *International Journal of Engineering Systems Modeling and Simulations*, 2(1-2):87–98, 2010.

[9] K.-D. Kantarakias, M.E. Chatzimanolakis, V.G. Asouti, and K.C. Giannakoglou. On the development of the 3D Euler equations using intrusive pce for uncertainty quantification. In *2nd ECCOMAS Thematic Conference on Uncertainty Quantification in Computational Sciences and Engineering (UNCECOMP 2017)*, Rhodes Island, Greece, June 15-17 2017.

[10] T. Ghisu and S. Shahpar. Towards affordable uncertainty quantification for industrial problems-Part I: Theory and validation. In *Proceedings of ASME Turbo Expo 2017, GT2017-64842*, Charlotte, NC, USA, June 26-30 2017.

[11] T. Ghisu and S. Shahpar. Towards affordable uncertainty quantification for industrial problems-Part II: Turbomachinery application. In *Proceedings of ASME Turbo Expo 2017, GT2017-64845*, Charlotte, NC, USA, June 26-30 2017.

[12] M. Emory, G. Iaccarino, and G.M. Laskowski. Uncertainty quantification in turbomachinery simulations. In *Proceedings of ASME Turbo Expo 2016, GT2016-56798*, Seoul, South Korea, June 13-17 2016.

[13] R. Abgrall, P.M. Congedo, S. Galera, and G. Geraci. Semi-intrusive and non-intrusive stochastic methods for aerospace applications. In *4th European Conference for Aerospace Sciences*, Saint Petersburg, Russia, July 4-8 2011.

[14] P.G. Constantine, A. Doostank, and G. Iaccarino. A hybrid collocation/Galerkin scheme for convective heat transfer problems with stochastic boundary conditions. *International Journal for Numerical Methods in Fluids*, 80:868–880, 2009.

[15] X. Chen, B. Ng, Y. Sun, and C. Tong. A flexible uncertainty quantification method for linearly coupled multi-physics systems. *Journal of Computational Physics*, 248:383–401, 2013.

[16] R. Duvigneau. Aerodynamic shape optimization with uncertain operating conditions using metamodels. RR-6143, INRIA, 2007.

[17] A.G. Liatsikouras, V.G. Asouti, K.C. Giannakoglou, G. Pierrot, and M. Megahed. Aerodynamic shape optimization under flow uncertainties using non-intrusive polynomial chaos and evolutionary algorithms. In *2nd ECCOMAS Thematic Conference on Uncertainty Quantification in Computational Sciences and Engineering (UNCECOMP 2017)*, Rhodes Island, Greece, June 15-17 2017.

[18] J. Miranda, D. Kumar, and C. Lacor. Adjoint-based robust optimization using polynomial chaos expansions. In *ECCOMAS Congress 2016, VII European Congress on Computational Methods in Applied Sciences and Engineering*, Crete island, Greece, June 5-10 2016.

[19] S. Shankaran and A. Jameson. Robust optimal control using polynomial chaos and adjoints for systems with uncertain inputs. In *20th AIAA Computational Fluid Dynamics Conference*, Hawaii, USA, June 27-30 2011.

[20] I.C. Kampolis, X.S. Trompoukis, V.G Asouti, and K.C. Giannakoglou. CFD-based analysis and two-level aerodynamic optimization on graphics processing units. *Computer Methods in Applied Mechanics and Engineering*, 199(9-12):712–722, 2010.

[21] O. Brodersen and A. Stürmer. Drag prediction of engine-airframe interference effects using unstructured Navier-Stokes calculations. In *16th AIAA Applied Aerodynamics Conference*, California, USA, June 11-14 2001.